Solid Freeform Fabrication 2024: Proceedings of the 35th Annual International Solid Freeform Fabrication Symposium – An Additive Manufacturing Conference
Reviewed Paper

STRATEGIZING SCAN TECHNIQUE SELECTION FOR COMPONENT REMANUFACTURING USING 3D PRINTING: A COMBINED REVERSE ENGINEERING AND TOPSIS BASED MULTI CRITERIA DECISION MAKING FRAMEWORK

Binoy Debnath*, Zahra Pourfarash*, Shivakumar Raman*, Hamidreza Samadi*

*Department of Industrial and Systems Engineering, The University of Oklahoma, Norman, OK 73019

Abstract

Remanufacturing mechanical components via reverse engineering and 3D printing is a promising alternative for sustainable manufacturing and prolonging part lifecycles. Selecting the right scanning method for reverse engineering is pivotal for ensuring remanufacturing accuracy, efficiency, and cost-effectiveness. This research proposes a pilot framework to assist decision-making in scanning method selection considering criteria such as scanning time, mesh repair time, digital model reconstruction time, 3D printing setup, printing & post processing, dimensional accuracy, and cost. Initially, non-contact-based methods such as laser scanning (Faro® scan arm), laser beam triangulation (Keyence® scanner) and structured light scanning (Artec Space Spider®) are employed to capture the component's geometry for CAD model development. Fused Deposition Modeling (FDM) 3D printing approach is then used to reproduce the part based on CAD models generated after each scanning method. The Technique for Order of Preference by Similarity to Ideal Solution (TOPSIS) is applied to determine the best scanning technique on the relative importance of criteria, allowing stakeholders to prioritize factors based on their needs. This structured approach enables strategic selection of the most suitable scanning technique for 3D printing mechanical component remanufacturing.

Keywords
3D Scanning, 3D Printing, Reverse Engineering, Scan Technique Selection

1. Introduction

Choosing the appropriate manufacturing process for a specific component is complex, involving factors to include process-material compatibility, shape complexity, dimensional accuracy, surface finish, and production volume; additionally, when redesigning obsolete parts, computer-aided design (CAD) models may be unavailable, nonexistent, or inconsistent with the current physical geometry (López & Vila, 2021). Reverse engineering (RE) involves analyzing and testing to recreate an object or event, serving as a reinvention technology for reconstructing and reproducing while preserving the original design intent. RE is utilized across numerous fields, such as aeropace industry, biomedical industries, and cultural heritage restoration, to create geometric models of objects that lack existence of CAD models (Kovács et al., 2015). RE is mainly used to duplicate unavailable OEM parts, repair or replace worn parts without original design data, and create models or prototypes for analysis using metrology, making it essential for producing mechanical components such as seals, O-rings, bolts, nuts, gaskets, and engine parts across various industries (Wang, 2010). The data acquisition process, or digitization, starts the Geometric Reverse Engineering by collecting surface data of components and transforming them into digital form; the precision of this initial step greatly influences the subsequent stages. Data acquisition methods are divided into contact and non-contact types (López & Vila, 2021). Devices such as Computed Tomography (CT) scanners, Magnetic Resonance Imagers (MRI), Ultrasonic Imaging apparatus, Photogrammetry, Stereoscopy, and Structured Light Scanners, Coordinate Measuring Machine (CMM), and Laser (Radar) or LiDar Scanners are used for 3D scanning and point cloud acquisition, thus playing a vital role in reverse engineering by collecting precise geometric data (Verim & Yumurtacı, 2020).

Engineering Design and Additive Manufacturing (AM) technologies significantly enhance business models by contributing to lifecycle management strategies, extending product life, and enabling more efficient production through the digitization of design and manufacturing processes (Kyaw et al., 2023). RE is a vital tool

for the successful execution of additive manufacturing, as it generates the precise geometry required for additive manufacturing systems to produce parts accurately (Macy, 2015).

Different studies have been conducted to RE and 3D print mechanical components using multiple techniques in literature. For instance, Paulic et al. (2014) employed optical scanning to reverse engineer the volume button component of a car and subsequently utilized selective laser sintering to produce a 3D-printed version of the part. Kyaw et al. (2023) demonstrated a strategic approach to RE using additive manufacturing technologies to support new business models for on-demand and decentralized manufacturing, comparing workflows of photogrammetry, laser scanning, and 3D re-modelling, and evaluating their cost, time, and quality for remanufacturing automobile parts using multi-criteria decision making (MCDM). However, no study is evident in applying decision making approaches for selecting the scan techniques.

2. Method

In this study, we chose a gasket for reverse engineering from a competition racing car. The gasket is vital for maintaining a tight seal between engine components, which prevents fluid and gas leaks and it ensures optimal engine performance. Accurately replicating and analyzing the gasket is crucial for the efficiency and reliability of the racing car. To accomplish this, we utilized two advanced scanning techniques: Probe and Laser Scanning (Faro) and Structured Light (SL) Scanning (Keyence®). The Faro scanner uses a laser line probe (LLP) to capture geometry from an object, through the use of a 7-axis arm. A beam is projected onto the object's surface, and a camera captures the beam location to measure points. Keyence® 3D scanners use a transmitter lens that projects structured light onto an object, and a receiver lens that detects the reflected light. The reflected light conforms to the surface topography, and uses triangulation to capture height. Both techniques are well-known for their accuracy and are quite frequently employed for object geometry capture. The gasket chosen is shown in Figure 1.

Figure 1: Selected gasket part of a car for the study

Initially, the gasket was scanned using both techniques to capture its precise geometry and surface details. The resulting scan data were then processed to create meshed files, which served as the foundation for reconstructing detailed CAD models. The reconstructed CAD models, based on the data obtained from Laser Scanning and Keyence® Scanning, were then utilized for manufacturing the gasket through 3D printing technology. This approach allowed us to compare the effectiveness and accuracy of both scanning methods in capturing the intricate features of the racing car gasket and producing high-fidelity replicas through additive manufacturing. Based on the selection criteria, the scanning methods were evaluated and ranked using the Technique for Order of Preference by Similarity to Ideal Solution (TOPSIS) method. This MCDM approach allowed us to systematically compare the performance of Laser Scanning and Keyence® Scanning against a set of predetermined criteria, ultimately determining which method best met the requirements for accurate gasket replication and analysis. The framework of the study is illustrated in Figure 2.

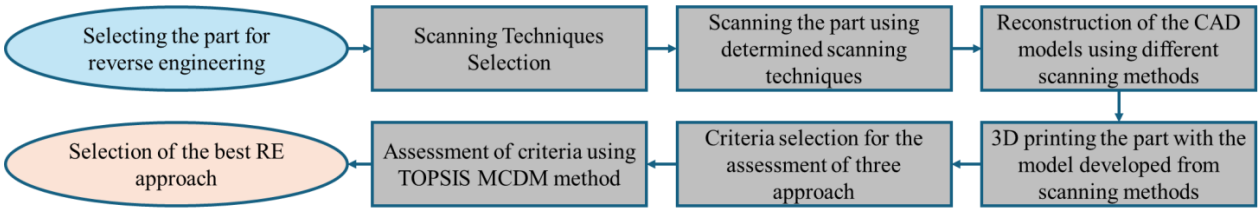

Figure 2: Framework of the study

2.1 Laser Scanning

In this study, we employed the Faro® scan arm as our laser scanning technique. The process begins by using the Faro® scan arm laser scanner to efficiently and precisely scan the gasket, capturing its surface geometry and creating point clouds. These point clouds are then used to generate a detailed 3D computer model of the gasket within the Geomagic Control X software. This software is instrumental in converting the scanned data into an accurate digital representation, enabling further analysis and reconstruction of the part. By leveraging the Faro® scan arm and Geomagic Control X, we ensured high precision in capturing the gasket's intricate details, facilitating its replication and study in the context of reverse engineering. The Faro® scan arm scanner used in this study is shown in Figure 3.


Figure 3: Faro® scan arm 3D laser scanner

The point cloud data generated from scanning the gasket part using the Faro® scan arm are captured through the live capture option of Geomagic Control X software. This live capture functionality ensures real-time acquisition of precise and detailed surface geometry of the gasket. Once the point cloud data is obtained, they are meticulously cleaned within the software to remove any noise or artifacts introduced during the scanning process. This cleaning step is crucial for enhancing the accuracy and quality of the data. Subsequently, the cleaned point cloud data is converted into a meshed file using the triangulate option in Geomagic Control X. This meshing process involves connecting the points to form a network of triangles, creating a detailed and continuous surface representation of the gasket. The resulting meshed STL file is then exported and imported into SolidWorks, where it serves as the foundation for developing a precise CAD model. In SolidWorks, the STL file is utilized to reconstruct the gasket's geometry with high accuracy. This CAD model development process includes refining the mesh, defining features, and ensuring that the model adheres to the exact specifications of the original part.

2.2 Laser beam triangulation

The research employed the Keyence® VL-770 laser scanner for comprehensive 3D surface scanning of parts, ensuring accurate reconstruction of intricate geometries. The Keyence® VL-770 is a high-precision 3D laser scanner that uses laser triangulation to capture detailed surface measurements. It projects a laser beam onto

an object's surface, and the reflected light is detected by sensors at a known angle. By measuring the reflection angle and the distance between the laser and sensors, the scanner calculates the exact position of each surface point. This process involves sweeping the laser across the object to collect a dense point cloud, which advanced software then processes into a detailed 3D model. The VL-770 is renowned for its high-resolution data acquisition, capturing even the finest surface details for applications like quality control and reverse engineering. This systematic approach enhanced the fidelity of digital reconstructions and broadened the potential uses of 3D scanning technology. The Keyence® scanner used in the study is shown in Figure 4.

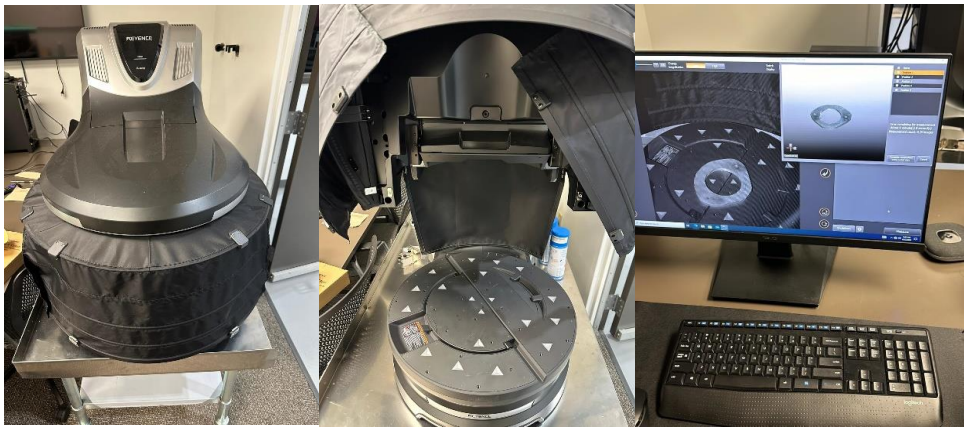

Figure 4: Keyence® VL-770 3D scanner

2.3 Structured Light Scanning

The study employed the Artec Space Spider® as a structured light scanning method, a handheld 3D scanner known for its high precision. Known for its accuracy, reliability, and capacity to capture fine details, the Artec Space Spider® excels at scanning small items or components with intricate shapes. It uses blue LED light to scan object surfaces, generating highly detailed and accurate 3D models. The Artec Space Spider® used in this study is located in the 3D scanning lab at the University of Oklahoma which is shown in Figure 5.

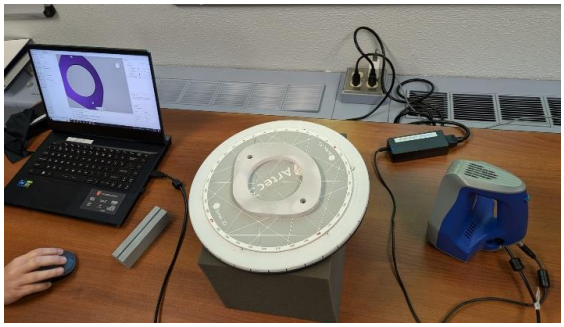

Figure 5: Artec Space Spider® 3D scanner

2.4 3D printing method

After scanning the part, post-processing is performed to create a solid CAD model suitable for 3D printing. The final CAD model is then converted into a binary STL file, which is used for slicing with PrusaSlicer. This slicing process generates G-code, the format compatible with the 3D printer. The 3D printer used in this study is a Prusa Mini, located at the Tom Love Innovation Hub facility at the University of Oklahoma. Figure 6 shows the 3D printer used in this study.

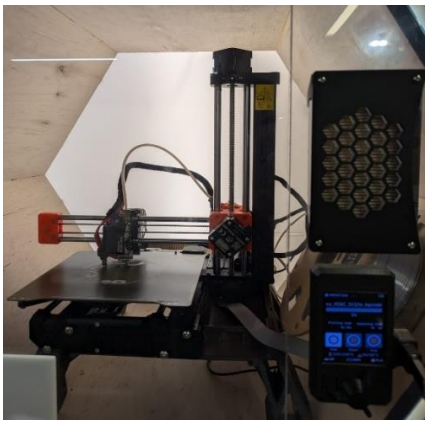

Figure 6: Prusa mini 3D printer

2.5 Criteria Selection

The criteria for analyzing scanning methods with the TOPSIS method include several essential factors. The criteria considered for the analysis are as follows:

1) Scan time: Scanning time refers to how long it takes to capture the complete geometry of the gasket.
2) Mesh repair time: Mesh repair time is the duration needed to clean and process the point cloud data, removing noise to create a usable mesh.
3) Digital CAD model reconstruction: Digital model reconstruction time involves converting the meshed data into a detailed CAD model.
4) 3D printing setup and slicing time: It includes preparing the 3D printer and slicing the digital model into printable layers.
5) Printing and post-processing time: It encompass the actual printing duration and any additional steps required to finish the printed part.
6) Part quality: Dimensional accuracy measures how closely the scanned and printed models match the original gasket dimensions.
7) Cost: It refers to the total expenses incurred throughout the process, including equipment, materials, and labor.

Evaluating these criteria with the TOPSIS method enables a comprehensive comparison of the scanning techniques, highlighting their strengths and weaknesses in the context of reverse engineering the gasket.

2.6 TOPSIS method

The TOPSIS (Technique for Order Preference by Similarity to Ideal Solution) method is a comprehensive multi-criteria decision-making technique that helps in selecting the most suitable alternative from a set of options. This method is particularly useful when decision-makers face complex scenarios involving multiple conflicting criteria. The stepwise procedure of TOPSIS method adopted from Sharma et al. (2018) is provided as follows:

1. **Creating the Decision Matrix (DM)**: The decision matrix is the foundational element of the TOPSIS method. It lists all the alternatives and the criteria that will influence the decision-making process. Each row in the matrix represents a different alternative, while each column corresponds to a specific criterion. This structured layout allows for a clear comparison of how each alternative measures up against each criterion.

2. **Normalizing Matrix (NM)**: Since the criteria often have different units and scales, the decision matrix needs to be normalized to make the criteria comparable. Normalization adjusts the values in the matrix to a common scale, typically between 0 and 1, ensuring that no criterion unduly influences the decision due to its scale. The normalized decision matrix (NDM) is calculated using the formula:

$$NM = R_{ij} = \frac{X_{ij}}{\sqrt{\sum_{i=1}^{m} X_{ij}^2}};$$

where Rij represents the original value in the decision matrix.

3. **Calculating the Weighted Decision Matrix**: Once the decision matrix is normalized, it is further refined by applying weights to each criterion. These weights reflect the relative importance of each criterion and are often determined using techniques such as the Analytical Hierarchy Process (AHP). By multiplying the normalized values by these weights, the weighted decision matrix (V) is obtained. The formula for this calculation is:

$$V = V_{ij} = R_{ij} * W_j,$$

where W_j represents the weight assigned to criterion j. This step ensures that the decision-making process aligns with the decision-maker's priorities and preferences.

4. **Determining the Positive and Negative Ideal Solutions**: The next step involves identifying the ideal solutions, which serve as benchmarks for comparison. The positive ideal solution (A^+) represents the best possible values for each criterion, while the negative ideal solution (A^-) represents the worst. For benefit criteria, the positive ideal solution is the maximum value in each column, and for cost criteria, it is the minimum value. Conversely, the negative ideal solution is the minimum value for benefit criteria and the maximum for cost criteria. These ideal solutions are calculated as follows:

$$PIS = A^+ = V_1, V_2, V_3, \dots\dots, V_n,$$
$$where\ V_j = \{(\max(V_{ij})\ if\ j \in B); (\min(V_{ij})\ if\ j \in C)\}$$
$$NIS = A^- = V_1^-, V_2^-, \dots\dots\dots, V_n^-,$$
$$where\ V_j = \{(\min(V_{ij})\ if\ j \in B);\ (\max(V_{ij})\ if\ j \in C)\}$$

Here, B indicates the beneficial criterion and C indicates the cost criterion.

5. **Calculating the Separation Measures (S_i^+ and S_i^-)**: To determine how close each alternative is to the ideal solutions, separation measures are calculated. S_i^+ represents the distance of an alternative from the positive ideal solution, while S_i^- represents the distance from the negative ideal solution. These distances are computed using the Euclidean distance formula:

$$S_i^+ = \sqrt{\sum_{j=1}^{n} V\left(V_j^+ - V_{ij}\right)^2};\ here, i = 1, 2, 3, \dots\dots, m$$

$$S_i^- = \sqrt{\sum_{j=1}^{n} V\left(V_j^- - V_{ij}\right)^2};\ here, i = 1, 2, 3, \dots\dots, m$$

These measures provide a quantitative basis for comparing the alternatives' performance relative to the ideal solutions.

6. **Calculating the Closeness Ratio (C_i)**: The closeness ratio (C_i) quantifies the relative proximity of each alternative to the ideal solutions. It is calculated as the ratio of the distance from the negative ideal solution to the total distance from both ideal solutions:

$$C_i^+ = \frac{S_i^-}{S_i^+ + S_i^-}$$

Here, $0 \leq C_i^+ \leq 1$. This ratio ranges between 0 and 1, where a higher value indicates that an alternative is closer to the positive ideal solution and thus more desirable.

7. **Ranking Based on Closeness Ratio**: Once the closeness ratios are calculated, the alternatives are ranked in descending order based on these values. The alternative with the highest closeness ratio is considered the closest to the ideal solution and is therefore the most preferred option.

8. **Final Ranking and Decision**: The final step involves making the decision based on the ranked alternatives. The alternative with a closeness ratio nearest to 1 is identified as the best choice, offering the optimal balance among the criteria considered. Conversely, an alternative with a closeness ratio closer to 0 is deemed the least favorable.

By meticulously following these steps, the TOPSIS method provides a structured and systematic framework for decision-making. This approach allows decision-makers to objectively evaluate, and rank alternatives based on their similarity to the ideal solutions, ensuring a transparent and rational selection process.

3. Result & Discussion

The gasket was scanned using three distinct 3D scanning techniques: laser scanning (Faro® scan arm), laser triangulation (Keyence®), and structured light scanning (Artec Space Spider®). Each technique captured the gasket differently, and the resulting outcomes are analyzed and discussed.

Figure 7(a) illustrates the scanned part obtained using the Faro® scan arm, shown after noise removal during the scanning process. The cleaned scan data is then triangulated using Geomagic Control X software and converted into an STL file for further CAD model construction. Using Fusion 360 and SolidWorks CAD software, the STL file is utilized to reconstruct a solid CAD model. This CAD model is subsequently used for 3D printing with a Prusa Mini 3D printer. The final solid CAD model developed is represented in Figure 7(b). The 3D printed part using the Prusa mini printer from CAD model reconstructed with Faro® scan arm scanning is shown in Figure 8.

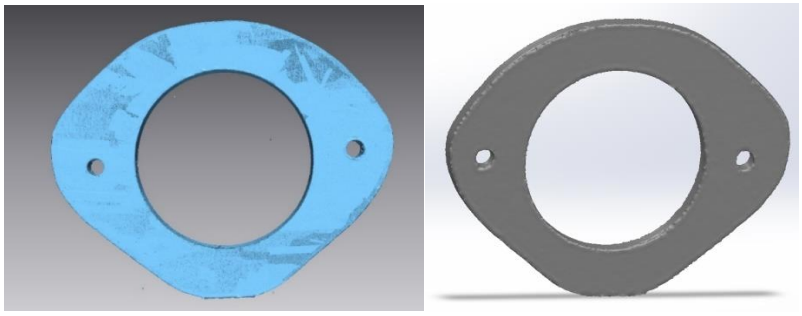

(a) (b)

Figure 7: (a) Scanned gasket part using Faro® scan arm; (b) CAD model conversion

Figure 8: 3D printed part from Faro® scan arm scanning method

The Keyence® scanning is performed on each facet from 6 to 8 angles, minimizing occlusions and ensuring thorough data coverage while mitigating shadowing effects as shown in Figure 9. The advanced laser technology facilitated precise measurement and high-resolution data acquisition, capturing even minute surface details. Post-scanning, the collected data sets were meticulously integrated using advanced software, aligning and merging individual scans to create seamless 3D models. The solid 3D model developed from Keyence® scanning is represented in Figure 10.

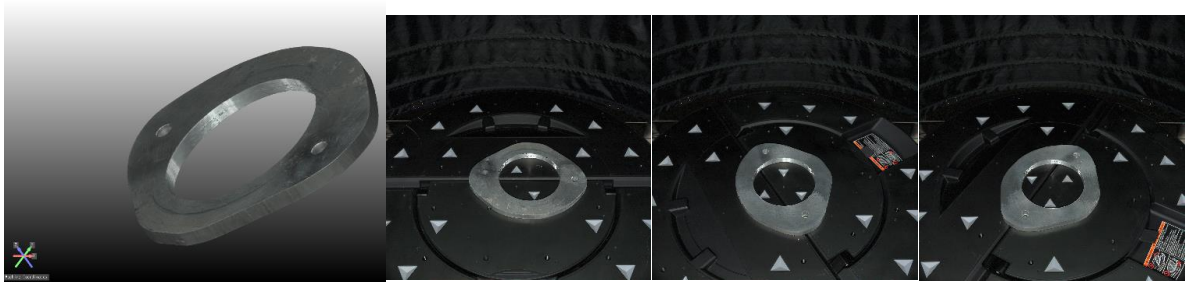

Figure 9: Scanning the gasket using Keyence®

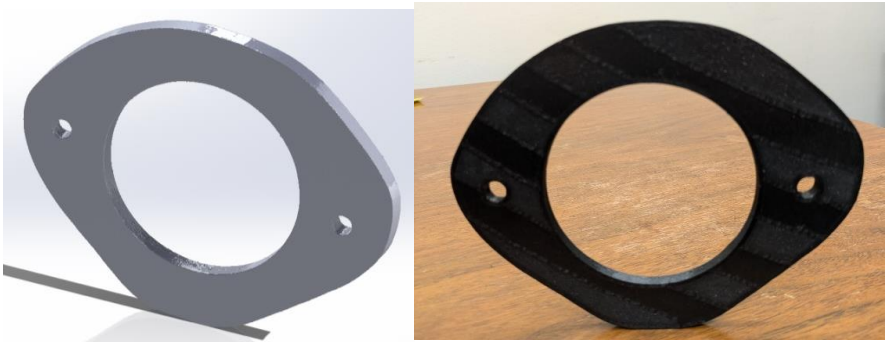

Figure 10: Solid model representation from Keyence® scanning

The Artec Space Spider® scanner was used to make another 3D scanning of the part. The scanned part is illustrated in Figure 11. Moreover, the solid CAD model representation and 3D printed part from that CAD model is represented in Figures 12(a) and 12(b) respectively.

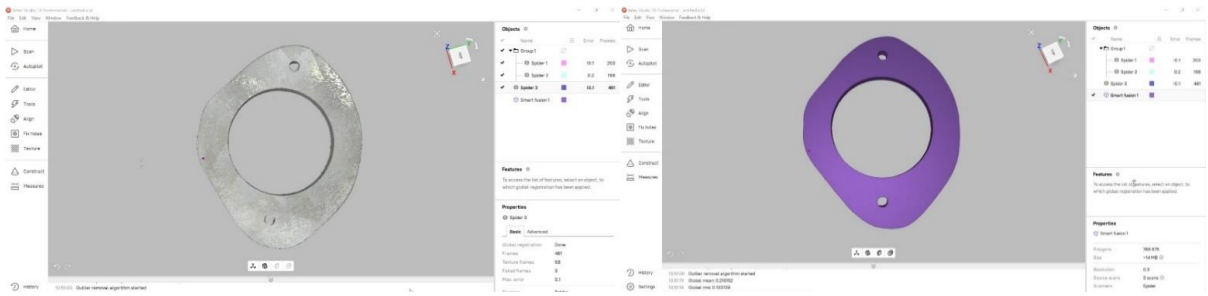

Figure 11: Scanned part in Artec Space Spider®

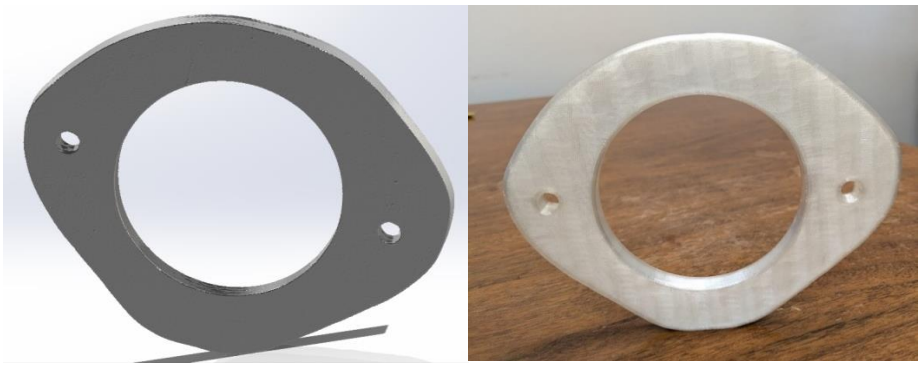

(a) (b)

Figure 12: (a) Solid CAD model from Artec Space Spider® scanning (b) 3D printed part

Now, for choosing the scanning technique, we applied the TOPSIS method to do the ranking. Firstly, the decision matrix is formed with different criteria. Here, the weight for each criterion is kept the same here as 0.1429 equally distributed between 7 criteria. The decision matrix of the criteria and the scanning technique alternatives are provided in Table 1.

Table 1: Decision matrix of criteria

Merged Decision Matrix							
Criteria	**Scanning time (Min)**	**Mesh Repair time (Min)**	**Digital model reconstruction time (Min)**	**3D printing setup time (Min)**	**Printing & Post Processing (Min)**	**Dimension accuracy (%)**	**Cost**
Weight	**0.1429**	**0.1429**	**0.1429**	**0.1429**	**0.1429**	**0.1429**	**0.1429**
Type	**Non-Ben**	**Non-Ben**	**Non-Ben**	**Non-Ben**	**Non-Ben**	**Ben**	**Non-Ben**
Faro® scan arm	80	40	40	30	300	99.4	360
Arctec	50	60	45	30	310	99.6	400
Keyence®	70	50	35	30	298	98.8	380
Sum square root	117.473	87.750	69.642	51.962	524.313	172.51	658.79

The values in Table 1 are based on a single observation for each scanning technique. While this provides an initial assessment of scanner performance, we recognize the importance of statistical rigor and conducting multiple trials to ensure the reliability of the results. Single observations, though sufficient for initial studies, will be expanded to include more observations, ensuring the data reflects true variability in scanner performance. Although the 3D printing setup time appears similar across all scanning techniques, its inclusion is essential to provide a comprehensive, end-to-end evaluation of the remanufacturing process. Even slight variations in setup can influence overall efficiency, especially in high-volume manufacturing environments. The quality of the scan data also affects how easily it integrates into the slicing process for 3D printing, potentially impacting the time required to prepare the model for printing. This criterion ensures that the analysis covers all aspects of the production workflow, not just the scanning phase. The difference in printing times (~12 minutes) stems from variations in the quality of the scan data produced by each scanner. Scanners that generate higher-fidelity, more detailed scans (e.g., Faro) may require additional time during the slicing and printing stages due to higher data complexity. Conversely, the Keyence scanner, with optimized surface data and fewer mesh errors, reduces the

time needed for G-code generation and subsequent printing. These discrepancies highlight how scanner quality impacts the efficiency of downstream processes, demonstrating that scanning performance directly influences printing time and overall workflow productivity.

Then, the decision matrix is converted to normalized matrix as presented in Table 2.

Table 2: Normalization of decision matrix

Criteria	Scanning time (Min)	Mesh Repair time (Min)	Digital model reconstruction time (Min)	3D printing setup time (Min)	Printing & Post Processing (Min)	Dimension accuracy	Cost
Weight	**0.1429**	**0.1429**	**0.1429**	**0.1429**	**0.1429**	**0.1429**	**0.1429**
Type	**Non-Ben**	**Non-Ben**	**Non-Ben**	**Non-Ben**	**Non-Ben**	**Ben**	**Non-Ben**
Faro® scan arm	0.681	0.456	0.574	0.577	0.572	0.576	0.546
Arctec	0.426	0.684	0.646	0.577	0.591	0.577	0.607
Keyence®	0.596	0.570	0.503	0.577	0.568	0.579	0.577

The normalized matrix is used to calculate the weighted decision matrix by applying the weights of each criterion. The weighted decision matrix is presented in Table 3, which also includes the ideal solutions, and separation measures. These ideal solutions are determined based on whether the criteria are beneficial or non-beneficial. In this context, dimensional accuracy is the only beneficial criterion, as higher accuracy is preferred. Conversely, cost and time are non-beneficial criteria, where lower values are more desirable. Moreover, the separation measures calculated indicate the closeness of alternative to ideal solutions.

Table 3: Weighted decision matrix

Criteria	Scanning time (Min)	Mesh Repair time (Min)	Digital model reconstruction time (Min)	3D printing setup time (Min)	Printing & Post Processing (Min)	Dimension accuracy	Cost		
Weight	**0.1429**	**0.1429**	**0.1429**	**0.1429**	**0.1429**	**0.1429**	**0.1429**		
Type	**Non-Ben**	**Non-Ben**	**Non-Ben**	**Non-Ben**	**Non-Ben**	**Ben**	**Non-Ben**	**S+**	**S-**
Faro® scan arm	0.0973	0.0651	0.0821	0.0825	0.0817	0.0823	0.078	0.038	0.035
Arctec	0.0608	0.0977	0.0923	0.0825	0.0845	0.0825	0.087	0.040	0.036
Keyence®	0.0851	0.0814	0.0718	0.0825	0.0812	0.0826	0.082	0.030	0.029
V+	0.0608	0.0651	0.0718	0.0825	0.0812	0.0826	0.078		
V-	0.0973	0.0977	0.0923	0.0825	0.0845	0.0823	0.087		

Now, the final ranking is presented in Table 4 based on the closeness ratio which is calculated with the positive and negative separation measures.

Table 4: Ranking of criteria

Criteria	S+	S-	(S+) + (S-)	Ci+	Rank
Faro® scan arm	0.0379	0.0353	0.0732	0.4824	2

Artec	0.0396	0.0365	0.0761	0.4796	3
Keyence®	0.0296	0.0294	0.0590	0.4983	1

These rankings highlight the superior performance of Keyence® scanning in this particular study, demonstrating its effectiveness in achieving accurate results. However, it is important to note that these rankings may change with variations in the parts being scanned and the complexity of those parts. Factors such as the size, geometry, material properties, and specific requirements of the scanning task can influence the effectiveness of each scanning method. Therefore, while Keyence® scanning currently holds the top position, the relative performance of each scanning technology should be reassessed when applied to different scenarios or more complex objects. This ensures that the most suitable scanning method is chosen for each specific application, optimizing accuracy and efficiency.

Moreover, it is valid that the performance differences between scanners in Table 4 appear marginal. However, the ranking remains valuable for several reasons, especially when considering the practical implications in real-world remanufacturing contexts. Small differences in scan time, accuracy, or mesh repair time can accumulate over multiple parts, leading to significant gains in efficiency and cost reduction, especially in high-volume remanufacturing scenarios. Moreover, the TOPSIS method allows decision-makers to adjust criteria weights based on their specific needs (e.g., prioritizing accuracy over cost), ensuring the ranking remains adaptable to different industrial contexts. While these scanners performed similarly for a gasket, larger or more complex geometries could reveal more substantial differences, making the ranking system essential for selecting the best scanner for specific tasks. In industries such as aerospace, defense, or medical device manufacturing, the slightest improvement in dimensional accuracy or fidelity can mean the difference between meeting or failing regulatory compliance. In these contexts, ranking the scanners even when their performance is close helps pinpoint which one best meets stringent tolerances.

While the general performance differences between scanning techniques are recognized, the novelty of this work lies in the strategic application of the TOPSIS-based decision-making framework to address the specific challenge of selecting the optimal scan technique for remanufacturing using RE and 3D printing. Although scanning technologies have been studied for RE and remanufacturing, no prior work has systematically applied TOPSIS to assess the best scanning method based on multiple practical criteria. Our study considers not only isolated criteria like accuracy but also the integration of scanning techniques into a full manufacturing process, including how captured data influences 3D printing efficiency. This holistic approach provides highly practical insights for optimizing the remanufacturing workflow. Our framework supports the goal of extending the lifecycle of obsolete or damaged parts by enabling accurate reverse engineering. In many cases, remanufacturers face the challenge of reproducing parts for which no CAD models exist. This study provides them with a decision-making tool to select the optimal scanning technology for recreating these parts with precision and cost-effectiveness, extending the lifecycle of components and reducing the need for new manufacturing. Few studies have approached scan technique selection using a formal multi-criteria decision-making model that includes both technical and economic factors. The framework of the study fills this gap, providing a base for future research and practical applications in RE and AM.

4. Conclusion

This study provided an evaluation of three 3D scanning technologies: Keyence®, Faro® scan arm, and Artec Space Spider® determining Keyence® as the top performer with a closeness ratio of 0.4992, followed by Faro® scan arm at 0.4827 and Artec Space Spider® at 0.4791. These findings underscore the critical importance of selecting the most suitable scanning technology based on specific task requirements, given the significant impact of part size, geometry, and complexity on scanner performance. However, the study had several limitations. The controlled environment may not reflect real-world conditions, where factors like lighting, surface texture, and ambient temperature can affect accuracy. The focus on a limited number of technologies and specific parts may overlook other potential high-performing scanners and part types. Future research should address these limitations by including a broader range of scanning technologies and parts with diverse and complex geometries. Studies should be conducted in varied real-world environments to understand the impact of different conditions

on scanning performance. Incorporating additional evaluation criteria such as user-friendliness, operational efficiency, and cost-effectiveness would provide a more comprehensive assessment. It is also essential to explore the impact of part complexity, size, and design on scanner performance. Applying varying weights to the evaluation criteria could reflect their real-world importance more accurately. Utilizing a hybrid Multi-Criteria Decision-Making (MCDM) approach could further refine the evaluation process. Moreover, the cost criteria are based on an estimated number of man-hours, which can be further evaluated in a more robust and precise manner. Collaborative efforts with industry partners could lead to tailored scanning solutions, enhancing the overall performance and applicability of 3D scanning technologies across different fields.

Acknowledgements

We sincerely acknowledge and appreciate the invaluable support and resources provided by the following entities:

- The Tom Love Innovation Hub at the University of Oklahoma, for granting access to their 3D printing facilities.
- The Rawl Engineering Practice Facility at the University of Oklahoma, for providing access to their state-of-the-art manufacturing facilities.
- The 3D Scanning Lab at OU Libraries, University of Oklahoma, for their expert assistance and access to structured light scanning techniques, which were instrumental in our research.

Their contributions played a crucial role in the successful completion of this study.

References

Sharma, A., Mukherjee Mondal, P., Naskar, S. K., & Haldar, A. (2018). Case study on automated inspection system selection using TOPSIS method. In *6th International Conference on Business Analytics and Intelligence (ICBAI-2018)* (pp. 165-170).

Kyaw, A. C., Nagengast, N., Usma-Mansfield, C., & Fuss, F. K. (2023). A Combined Reverse Engineering and Multi-Criteria Decision-Making Approach for Remanufacturing a Classic Car Part. *Procedia CIRP*, *119*, 222-228.

Paulic, M., Irgolic, T., Balic, J., Cus, F., Cupar, A., Brajlih, T., & Drstvensek, I. (2014). Reverse engineering of parts with optical scanning and additive manufacturing. *Procedia engineering*, *69*, 795-803.

López, J., & Vila, C. (2021, October). An approach to reverse engineering methodology for part reconstruction with additive manufacturing. In *IOP conference series: materials science and engineering* (Vol. 1193, No. 1, p. 012047). IOP Publishing.

Macy, B. (2015). Reverse engineering for additive manufacturing. In *Handbook of manufacturing engineering and technology* (pp. 2485-2504). Springer, London.

Kovács, I., Várady, T., & Salvi, P. (2015). Applying geometric constraints for perfecting CAD models in reverse engineering. *Graphical Models*, *82*, 44-57.

Verim, Ö., & Yumurtacı, M. (2020). Application of reverse engineering approach on a damaged mechanical part. *International Advanced Researches and Engineering Journal*, *4*(1), 21-28.

Wang, W. (2010). *Reverse engineering: Technology of reinvention*. Crc Press.

Kyaw, A. C., Nagengast, N., Usma-Mansfield, C., & Fuss, F. K. (2023). A Combined Reverse Engineering and Multi-Criteria Decision-Making Approach for Remanufacturing a Classic Car Part. *Procedia CIRP*, *119*, 222-228.